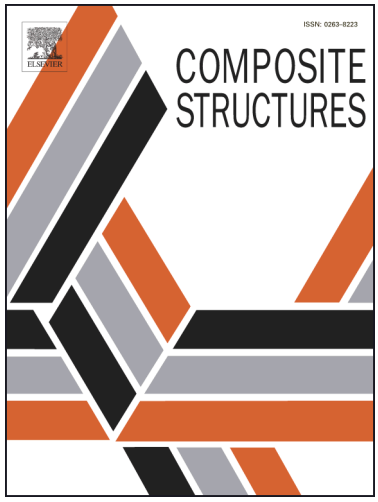

Nanocellulose coated woven jute/green epoxy composites: Characterization of mechanical and dynamic mechanical behavior

Abdul Jabbar, Jiř í Militký, Jakub Wiener, Bandu Madhukar Kale, Usman Ali, Samson Rwawiire

PII: S0263-8223(16)31996-1
DOI: http://dx.doi.org/10.1016/j.compstruct.2016.11.062
Reference: COST 8023

To appear in: *Composite Structures*

Received Date: 5 September 2016
Revised Date: 15 November 2016
Accepted Date: 18 November 2016

Please cite this article as: Jabbar, A., Militký, J., Wiener, J., Madhukar Kale, B., Ali, U., Rwawiire, S., Nanocellulose coated woven jute/green epoxy composites: Characterization of mechanical and dynamic mechanical behavior, *Composite Structures* (2016), doi: http://dx.doi.org/10.1016/j.compstruct.2016.11.062

Nanocellulose coated woven jute/green epoxy composites: Characterization of mechanical and dynamic mechanical behavior

Abdul Jabbar[a, *], Jiří Militký[a], Jakub Wiener[a], Bandu Madhukar Kale[a], Usman Ali[b], Samson Rwawiire[a],

[a]Department of Material Engineering, Technical University of Liberec, Studentská 2, 461 17 Liberec, Czechia

[b]BZU College of Textile Engineering, Multan Pakistan

[*]Corresponding author. E-mail: abduljabbarntu@gmail.com

Phone: +420 48 535 3228

Abstract

This paper presents the preparation and characterization of nanocellulose coated woven jute/green epoxy composites. Waste jute fibers were used as precursor to purify and extract nanocellulose by chemical treatments. The prepared suspensions with 3, 5 and 10 wt% of nanocellulose were coated over jute fabric followed by preparation of composites by compression molding technique. The surface morphologies of treated jute fibers, jute cellulose nanofibrils (CNF), nanocellulose coated jute fabrics and fractured surfaces of composites were characterized by scanning electron microscopy (SEM). The crystallinity of jute fibers after different chemical treatments was measured by X-ray diffraction (XRD). The effect of nanocellulose coating over jute reinforcement on the tensile, flexural, fracture toughness and dynamic mechanical properties of prepared composites has been investigated. Fracture toughness was measured using single end notched bend (SENB) specimens and dynamic mechanical test was performed in three point bending mode. The results revealed the improvement in tensile

modulus, flexural properties and fracture toughness except the decrease in tensile strength of nanocellulose coated woven jute/green epoxy composites as compared to uncoated jute composite. Dynamic mechanical analysis (DMA) results also showed the increase in storage modulus and reduction in tangent delta peak height of nanocellulose coated jute composites.

Keywords: Jute fibers, nanocellulose coating, mechanical properties, fracture toughness, dynamic mechanical analysis

1. Introduction

Natural fiber reinforced polymer composites (NFPC) have gained considerable attention in the recent years due to their environment and economic benefits and low energy consumption [1, 2]. Natural fibers offer many advantages over their synthetic counterparts (e.g. glass and carbon) such as cost effectiveness, light weight, easy to process, renewable, recyclable, available in huge quantities, low fossil-fuel energy requirements and the most importantly their high specific strength to weight ratio [1, 3]. Thus natural fibers are considered promising candidates for replacing conventional synthetic reinforcing fibers in composites for semi-structural and structural applications [4].

Cellulose is an abundant, renewable and biodegradable naturally occurring material on earth that can be obtained from numerous resources [5]. It is an infinite source of raw material for environment friendly and biocompatible products. Lignocellulosic fibers such as jute, hemp and flax etc. are rich in cellulose, abundantly available and easy to handle and process. Cellulose micro/nano fillers in polymers have already attracted considerable interest by improving the strength and stiffness of resulting composites [5-7]. Various types of cellulosic resources are used as precursors to extract and purify cellulose fibrils from lignocellulosic fibers. In the

previous literature, cellulose micro/nano fibrils obtained from different precursors such as hemp fibers [8], pineapple [9], isora fibers [5] and jute fibers [10] are used as reinforcing filler in polymer matrices and resulted in the improvement of composite properties. However, in the present study, waste jute fibers are used as precursor to extract and purify nanocellulose which is subsequently coated over the woven jute fabric instead of using it as filler in matrix. Afterwards, the nanocellulose coated jute fabric is used as reinforcement in green epoxy polymer to form a composite material. Therefore, the objective of the present study is to characterize the mechanical and dynamic mechanical properties of composites reinforced with nanocellulose coated jute fabric. To the author's best knowledge, there is no study available in open literature yet that fulfills the above mentioned objective using nanocellulose coated jute fabric as reinforcement and green epoxy resin as matrix system.

2. Materials and methods

2.1.Material

Woven jute fabric produced from tossa jute (*C. olitorius*) fibers having an areal density of 600 gm^{-2} with 5-end satin weave design was produced on a shuttle loom with 386 tex yarn. Warp and weft densities of the fabric were 6.3 threads per cm and 7.9 threads per cm respectively. Waste jute fibers, sourced from a jute mill, were used as precursor for purification and extraction of nanocellulose. Green epoxy resin CHS-Epoxy G520 and hardener TELALIT 0600 were supplied by Spolchemie, Czech Republic. The main characteristics of the resin system are reported in our previous study [11]. Sulphuric acid (H_2SO_4) and sodium hydroxide (NaOH) were supplied by Lach-Ner, Czech Republic. Sodium sulfate (Na_2SO_4) and sodium hypochlorite (NaOCl) were supplied by Sigma-Aldrich, Czech Republic.

2.2.Purification and extraction of nanocellulose from waste jute fibers

Waste jute fibers were chopped to approximate length of 5-10 mm and immersed in 2 % sodium hydroxide (NaOH) solution for 2 h at 80 ˚C temperature maintaining a liquor ratio of 50:1. The process was repeated three times. The fibers were then washed with tap water several times to remove any traces of NaOH sticking to the fibers surface. The jute fibers were then bleached with 7.0 g/l sodium hypochlorite (NaOCl) solution at room temperature for 2 h under pH 10-11 and subsequently antichlored with 0.1 % sodium sulphate (Na_2SO_4) at 50 °C for 20 min. Finally, the fibers were washed with tap water several times until the final pH was maintained at 7.0 and then allowed to dry at room temperature for 48 h and at 100 °C in an oven for 2 h. Alkali and bleaching treatments were used to purify cellulose and to remove maximum amount of hemicellulose and lignin from the fibers. The bleached jute fibers were milled using a high-energy planetary ball mill of Fritsch pulverisette 7. Milling process relies on the principle of energy release at the point of impact between balls as well as on the high grinding action created by friction of balls on the wall [12]. The sintered corundum container of 80 ml capacity and zirconium balls of 10 mm diameter were chosen for 20 min of milling. The ball to material ratio (BMR) was kept at 10:1 and the speed was kept at 850 rpm. Acid hydrolysis of milled jute fibers was conducted for 1 hour at 45 °C under mechanical stirring using 65 % (w/w) H_2SO_4. The fiber content during acid hydrolysis was 5 % (w/w). The amorphous regions are preferably attacked by acids while crystalline regions are mostly insoluble in acids. The basic principle of acid hydrolysis is to release hydronium ions (H^+) for hydrolytic cleavage of glycosidic bonds in cellulose molecular chains within amorphous regions along the cellulose nanofibrils (CNF), thereby breaking the hierarchical structure of the fibril bundles into crystalline CNF [13]. After the hydrolysis, the suspension was diluted with cold water (4 °C) to stop the reaction, neutralized

with NaOH solution and discolored by NaOCl solution. The supernatant was removed from the sediment and replaced by new distilled water several times. Finally, 3 %, 5 % and 10 % (w/w) nanocellulose suspensions were prepared by increasing cellulose concentration and decreasing water concentration through vacuum filtration using Buchner funnel.

2.3.Coating of jute fabric with nanocellulose

The prepared nanocellulose suspensions (3, 5, and 10 wt %) were ultasonicated for 5 min with Bandelin ultrasonic probe and then applied on the surface of jute fabric by roller padding at room temperature. Finally, the coated fabrics were dried at 70 °C for 60 min.

2.4.Preparation of composites

The composites were prepared by hand layup method. The resin and hardener were mixed in a ratio of 100:32 (by weight) according to manufacturer recommendations, before hand-layup. The prepared resin mixture was poured on fabric layers and spread out by a hand roller. The gentle rolling action of hand roller confirmed the wetting of jute fabrics and the excess resin was squeezed out of the panel layup by the roller. The composite layup along with Teflon sheets were sandwiched between a pair of steel plates and cured at 120 °C for 1.0 h in mechanical convection oven with predetermined weight on it to maintain uniform pressure of about 50 kPa [11]. The fiber volume fraction (V_f) of all composites was in the range of 0.25-0.27. The prepared composite samples were designated as CF0 (uncoated), CF3 (3 wt % nanocellulose coated), CF5 (5 wt % nanocellulose coated) and CF10 (10 wt % nanocellulose coated).

2.5.Characterization and testing

2.5.1. Scanning electron microscopy (SEM)

The morphologies of alkali treated and bleached jute fibers, cellulose nanofibrils and nanocellulose coated jute fabrics were observed with Vega-Tescan TS5130 Scanning Electron

Microscope at 30 kV accelerating voltage. The surface of fibers was gold coated prior to SEM inspection. Additionally, in order to measure the size distribution using SEM image, the morphology of cellulose nanofibrils was also observed on Zeiss Ultra Plus field emission scanning electron microscope (FE-SEM) at low accelerating voltage (1.0 kV) and low probe current (≈ 10 pA) to eliminate charging effect and sample damage due to interaction with primary electrons. The software used for image analysis was NIS Elements BR 3.22.

2.5.2. X-ray diffraction (XRD)

X-ray diffraction patterns were recorded on a PANalytical X′ Pert PRO MPD diffraction system for untreated jute, bleached jute and jute cellulose nanofibrils in order to examine the change in crystallinity of the material after bleaching and acid hydrolysis**.**

2.5.3. Mechanical characterization of composites

Tensile properties of the composites were characterized on an MTS series 370 servo-hydraulic load frame equipped with 647 hydraulic wedge grip of 100 kN load capacity at a cross head speed of 2 mm/min and gauge length of 100 mm in accordance with ASTM D3039-00 using rectangular specimens of dimension 200×20×h mm^3, where "h" is the actual thickness of specimen in the range of 4.0 to 4.5 mm. Flexural test was performed in three point bending mode on a universal mechanical testing machine, Shimadzu AGS-J with 5kN load cell, following ASTM D790 standard at a cross head speed of 2.0 mm/min. The specimens of dimension 160×12.7×h mm^3 were used maintaining a span to thickness ratio of 32:1 according to standard recommendations ("h" is the actual thickness of specimen in the range of 4.0 to 4.5 mm).

Fracture toughness, K_{Ic}, of composites was determined by three point bending method using the single edge notch bend (SENB) specimens in accordance with the standard test method ASTM D5045-99. A sharp crack of length "*a*" between 0.45 W and 0.55 W was introduced by using a

notch maker CEAST NOTCHVIS and a fresh razor blade at the notch tip ('W' is the width of specimen). The specifications of fixture and specimens are shown in Fig. 1. The tests were performed using universal mechanical testing machine, Shimadzu AGS-J with 5 kN load cell, at a cross head speed of 10 mm/min. The K_{Ic} values were determined using the following relationship recommended by testing standard:

$$K_Q = \left(\frac{P_Q}{BW^{1/2}}\right) f(x), \quad W = 2B \tag{1}$$

$$f(x) = 6x^{1/2}\frac{[1.99 - x(1-x)(2.15 - 3.93x + 2.7x^2)]}{(1+2x)(1-x)^{3/2}}, \quad x = {}^{a}/_{W} \tag{2}$$

$$B, a, W - a \geq 2.5\left(\frac{K_Q}{\sigma_{YS}}\right)^2 \tag{3}$$

where K_Q is a provisional fracture toughness, f the shape factor, P_Q the peak load, B the specimen thickness , W the specimen width, a the crack length, σ_{YS} the yield strength. Eq. 3 was satisfied for the dimensions of fabricated SENB specimens. The fractured surfaces of composites were characterized by Vega-Tescan TS5130 SEM. Statistical analysis of tensile, flexural and fracture toughness properties was done by one-way analysis of variance (ANOVA) and probability value $p \leq 0.05$ was considered as an indicative of statistical significance compared to the control sample (CF0 composite).

2.5.4. Dynamic mechanical characterization

The dynamic mechanical properties of composites were measured in 3-point bending mode using Q800 Dynamic Mechanical Analysis (DMA) instrument of TA instruments (New Castle DL, USA). The testing conditions were controlled in the temperature range of 30–180 °C, with a heating rate of 3 °C/min, fixed frequency of 1 Hz, preload of 0.1 N, amplitude of 20 µm, and force track of 125%. The samples having a thickness of 4–4.5 mm, width of 12 mm and span

length of 50 mm were used for DMA. Two replicate samples were tested for each condition and average values are reported.

3. Results and Discussion

3.1.Surface morphology of treated jute fibers and jute cellulose nanofibrils

Surface morphologies of jute fibers after alkali treatment, bleaching and milling and cellulose nanofibrils after acid hydrolysis are examined by SEM and presented in Fig. 2. Fig. 2a shows the jute fibers bound together in the form of fiber bundles by cementing materials e.g. hemicellulose and lignin but after repeated alkali treatment, splitting of fibers is observed due to destruction of mesh structure with a little rough and clean surface, may be due to majority of the removal of hemicellulose, lignin and other non-cellulosic materials [14, 15] as shown in Fig. 2b.

The alkali treated fibers are further separated to individual fibers with more clean surface and fibrillation on the surface, may be due to more delignification after bleaching treatment [16], as shown in Fig. 2c. Fig. 2d displays the milled jute fibers with size distribution of fibers in the micron range but after acid hydrolysis of milled fibers, one can recognize cellulose nanofibrils with distribution of diameter in nanometer range (Fig. 2e, f). A high resolution FE-SEM image at nanoscale level is precisely analyzed to measure the size (diameter) of jute CNF as shown in Fig 3a. The histogram of size distribution of 50 measurements is shown in Fig. 3b. The calculated average diameter of CNF was found to be 57.40 ± 20.61 nm.

3.2.Surface morphology of nanocellulose coated jute fabric

The morphological changes that occur on the surface of jute fabric after nanocellulose coating are shown in Fig. 4. It is apparent that there is depositing of nanocellulose on the fabric surface forming a layer. The layer thickness increases gradually with the increase in nanocellulose

concentration as clear in Fig. 4b-d and the fabric surface coated with 10 wt % of nanocellulose suspension is covered almost completely with nanocellulose as shown in Fig. 4d.

3.3.XRD analysis of jute fibers

The X-ray diffraction patterns of untreated jute fibers, bleached jute fibers and jute CNF are shown in Fig 5. These diffraction patterns are typical of semicrystalline materials with an amorphous broad small hump and a large crystalline peak. Two well defined peaks around $2\theta \approx 16^{\circ}$ and 23° are typical of cellulose I. The crystallinity index for all samples was determined by using the following formula [17]:

$$Crystallinity\ \% = 100 \times \frac{I_{2\,0\,0} - I_{non-cr}}{I_{2\,0\,0}} \qquad (4)$$

Where $I_{2\,0\,0}$ represents maximum intensity of the peak corresponding to the plane 2 0 0 at 2θ angle between 22 – 24 degrees and $I_{non\text{-}cr}$ is the intensity for diffraction of non-crystalline material which is taken at 2θ angle of about 18 degree. The crystallinity index was calculated to be about 69.3 %, 76.5 % and 78.6 % for untreated fibers, bleached fibers and cellulose fibrils, respectively. The increase in crystallinity of bleached jute fibers as compared to untreated jute can be explained by the removal of amorphous non-cellulosic compounds induced by the alkali and bleaching treatments, performed to purify cellulose and that of jute CNF, by removal of amorphous cellulosic domains due to acid hydrolysis.

3.4.Tensile properties

Fig. 6a shows the typical stress-strain curves of uncoated and coated jute composites with different nanocellulose content. The stress-strain curve for uncoated (CF0) composite shows almost linear behavior until failure whereas the curves for composites coated with different

nanocellulose content show linear behavior followed by change in slope showing nonlinear behavior, thus presenting plastic deformation and gradual debonding of fibers from the matrix just before failure . The tensile failure behavior also reveals more brittle nature of CF0 composite as compared to nanocellulose coated composites (Fig. 6a).

Fig. 6b presents the average values and standard deviation of ultimate tensile strength and tensile modulus of composites. The tensile properties indicate decrease in strength and increase in modulus (stiffness) of composites with the increase in nanocellulose concentration. For CF10 composite, the tensile modulus increases from 4.6 GPa to 5.58 GPa showing 21 % increase, thus presenting better fiber/matrix interfacial interaction and bonding which would be effective at the early stages of loading. However, the decrease in tensile strength of composites with the increase in nanocellulose concentration may be explained by the differences in failure strains of nanocellulose coated jute fabric reinforcement and the matrix. In other words, the reinforcement does not come into effect when the failure strain of matrix is much greater than that of reinforcement. So the composite shows a failure before the stress is transferred from matrix to reinforcement [6]. The ANOVA for the tensile strength ($p = 0.000$) and tensile modulus ($p = 0.008$) showed the statistically significant difference between the means at the 95.0 % confidence interval.

3.5.Flexural properties

The flexural strength and modulus increase with the increase in nanocellulose concentration in composites. The flexural strength increases from 32.94 MPa for CF0 composite to 32.94 MPa, 43.53 MPa and 48.66 MPa for CF3, CF5 and CF10 composites respectively, thus allowing 26 %, 32 % and 47 % increase on average as shown in Fig. 7. Similarly, flexural modulus increases from 3.83 GPa for CF0 composite to 4.81 GPa, 4.73 GPa and 5.67 GPa for CF3, CF5 and CF10

composites respectively, thus permitting 25 %, 23.5 % and 48 % increase on average (Fig. 7). These findings may suggest the strong interaction between matrix and reinforcement after nanocellulose coating which increases with the increase in nanocellulose content. The other possibility of the enhancement of flexural properties may be the increase in bending stiffness/rigidity of jute reinforcement after coating with nanocellulose which also increases with the increase in its concentration [18, 19]. The ANOVA for the flexural strength (p = 0.000) and flexural modulus (p = 0.000) also showed the statistically significant difference between the means at the 95.0 % confidence interval.

3.6.Fracture toughness

Fig. 8a shows the typical K_Q vs. displacement curves presenting the crack growth behavior of composites and Fig. 8b presents the fracture toughness (K_{1c}) with respect to nanocellulose content in composites. The fracture mode was brittle for CF0 composite showing slip-stick behavior but as the nanocellulose content over jute reinforcement increased, the fracture mode changed from brittle to ductile and K_{1c} values increased from 2.64 MPa.m$^{1/2}$ for CF0 composite to 3.20 MPa.m$^{1/2}$, 3.21 MPa.m$^{1/2}$ and 3.49 MPa.m$^{1/2}$ for CF3, CF5 and CF10 composites respectively, resulting 21 %, 21.5 % and 32 % increase on average (Fig. 8b). Thus, fracture toughness increases linearly with the increase in concentration of nanocellulose coating over reinforcement. The ANOVA for the fracture toughness, K_{1c} (p = 0.024) showed the statistically significant difference between the means at the 95.0% confidence interval.

Crack deflection, plastic deformation, voids, crack pinning/bridging, fiber pullout and debonding are the known toughening mechanisms in epoxy matrices, found in literature [20]. Fig. 9a-d exhibits SEM images for all nanocellulose contents. Figures clearly show fiber fracture, fiber pullout and some voids for all composites. However, fiber pullout is a little more prominent

mechanism for nanocellulose coated composites, may be due to increased fiber debonding during fracture resulting in increased crack propagation length during deformation and hence fracture toughness.

Fig. 10 shows the fracture surface morphologies in the matrix region. It can be seen from Fig. 10a that the fracture surface of green epoxy matrix of CF0 composite is very smooth and featureless, which indicates typical brittle fracture behavior with lack of significant toughness mechanism [21]. However, Fig. 10b-d show rougher fracture surfaces and river patterns in the matrix regions of nanocellulose coated jute composites. An increase in fracture surface roughness can be used as an indicator to the presence of plastic deformation and crack deflection mechanisms, which increase fracture toughness by increasing crack propagation length during deformation [22].

3.7.Dynamic mechanical analysis (DMA)

The viscoelastic response of a material can be analyzed by dynamic mechanical analysis (DMA) and dynamic mechanical properties are expressed in terms of storage modulus, loss modulus (the energy dissipation associated with the motion of polymer chains) and loss factor or tan delta (ratio of loss modulus and storage modulus) of polymer composites within the measured temperature range [23]. Storage modulus (E') is the contribution of elastic components of a viscoelastic material and represents its stiffness. It is proportional to the energy stored during a loading cycle. The change in storage modulus as a function of temperature of different nanocellulose coated and uncoated jute composites is shown in Fig. 11. It can be seen that the shape of storage modulus curves is almost same for all the samples and E' decreases with increase in temperature because of the transition from glassy to rubbery state. However, the storage modulus increases with increasing concentration of nanocellulose in composites both in

glassy and rubbery regions showing superior reinforcing effects of nanocellulose coated jute fabrics throughout the specified temperature range. In the glassy region, components are highly immobile, close, tightly packed [24] and intermolecular forces are strong [25] resulting in high storage modulus but as temperature increases intermolecular forces become weak, the components become more mobile and lose their close packing arrangement, resulting in loss of stiffness and hence storage modulus. Fig. 11 reveals that uncoated jute composite (CF0) has the lowest storage modulus throughout the specified temperature range. CF0 has 4.05 GPa of E' (measured at 30 ˚C), however, CF3, CF5, CF10 composites show maximum values of 4.72, 5.27 and 6.35 GPa respectively resulting in an increase of 16 %, 30 % and 56 % in E'. Moreover, E' (measured at 150 ˚C) increased from 0.28 GPa for CF0 composite to 0.48, 0.71 and 0.94 GPa for CF3, CF5, CF10 composites respectively representing 71 %, 153 % and 235 % increase. This shows that when nanocellulose concentration over the jute fabric is increased, the stiffness effect of reinforcement is progressively increased not only in the glassy region but also in the rubbery region.

The variation of the storage modulus of composites at different temperatures is plotted and shown in Fig. 12. In all cases, the storage modulus of nanocellulose coated composites is higher than that of uncoated one, especially at higher temperatures. The above findings may be attributed to the fact that, as nanocellulose coated on jute fabric has large surface area, it promotes the interfacial interactions between the reinforcement and matrix thus reducing the mobility of polymer chains [26] and better stress transfer at the interface [27]. The other fact is the increase in the stiffness of reinforcement with increasing nanocellulose concentration. Furthermore, the formation of rigid and stiff network interconnected by hydrogen bonds is the

accepted theory to explain the excellent mechanical properties of composites incorporated with nanocellulose [28-31].

Fig. 13 presents the loss modulus (E'') versus temperature of different nanocellulose coated and uncoated jute composites. Loss modulus is the contribution viscous components of a material [32] and is indicative of energy dissipated as heat by the system during a deformation cycle due to viscous motions inside the material itself [33]. It is observed that the value of loss modulus increased and then decreased with the increase in temperature for all composites. The maximum heat dissipation occurs at the temperature at which the value of loss modulus is maximum, representing the glass transition temperature (T_g) of the system [34]. The rapid rise in loss modulus in a system indicates an increase in the polymer chains free movements at higher temperatures due to a relaxation process that allows greater amounts of motion along the chains that is not possible below the glass transition temperature [35]. Fig. 13 also revealed that the value of loss modulus is increased with the increase in concentration of nanocellulose coating as compared to uncoated composite (CF0) representing a higher amount of energy dissipation associated with an increase in internal friction.

T_g values obtained from loss modulus (E'') are considered to be more convincing as compared to those obtained from damping factor ($tan\ \delta$) [36]. It is interesting to note that T_g is decreased from 95 ˚C for CF0 composite to 88 ˚C and 91 ˚C for CF3 and CF5 composites respectively but T_g of CF0 and CF10 composites are almost same. Simultaneously, a positive shift in T_g values to higher temperatures is noted with the increase in nanocellulose concentration in the system (Table 1). A possible reason may be the change in crosslinking density of the network [37].

The ratio of loss modulus and storage modulus is known as the damping factor or $tan\ \delta$. In other words, it is the ratio of the energy dissipated to the energy stored during a dynamic loading

cycle. It provides the information about how good a material can absorb energy. The damping factor (*tan δ*) as a function of temperature of composites reinforced with different concentration of nanocellulose coated jute fabric is shown in Fig. 14. The highest value of *tan δ* peak is observed for CF0 composite resulting in more energy dissipation whereas a reduction is *tan δ* peak height is observed in composites with the increase in concentration of nanocellulose coating. The peak height of 0.59 for CF0 composite is reduced maximum to 0.42 for CF10 composite representing a 40 % decrease (Table 1) thus indicating that there are both strong intermolecular and physical interactions contributing to greater molecular restrictions at the interface and less energy dissipation and that the storage modulus is influenced more by the increase in nanocellulose concentration than loss modulus in the composites. The width of *tan δ* peak becomes broader for nanocellulose coated jute composites especially for CF5 and CF10. The damping in materials generally depends on the molecular motions at the interfacial region [38]. Therefore, the increase in width of *tan δ* peak of nanocellulose coated composites is suggestive of increased volume of interface [25] and an increase in the inhibition of relaxation processes in composites thus decreasing the mobility of polymer chains within the system and a higher number of chain segments upon increase in concentration of nanocellulose in composites [39].

4. Conclusion

The jute cellulose nanofibrils were successfully prepared and coated over woven jute reinforcement using three different concentrations (3, 5 and 10 wt %). The tensile, flexural, fracture toughness and dynamic mechanical properties of prepared nanocellulose coated woven jute/green epoxy composites were investigated subsequently. Tensile modulus, flexural strength, flexural modulus and fracture toughness of composites were found to improve with the increase

in concentration of nanocellulose coating over jute reinforcement except the decrease in tensile strength. Dynamic mechanical test also revealed the increase in storage modulus and reduction in tangent delta peak height of composites with the increase in nanocellulose concentration over jute reinforcement. Based on the analysis of results, the improvement in mechanical and dynamic properties were likely attributed to the increase in interfacial interaction between reinforcement and matrix due to large surface area exposed by nanocellulose coated over jute reinforcement, the formation of rigid and stiff network interconnected by hydrogen bonds and the increase in the stiffness of reinforcement with increasing nanocellulose concentration. Whereas, the differences in failure strains of coated jute reinforcement and the matrix might be the reason of reduction in tensile strength of these composites.

Acknowledgement

The authors acknowledge the financial support from Technical University of Liberec under student grant scheme (SGS-21158) to carry out this work.

References

[1] Jabbar A, Militký J, Kale BM, Rwawiire S, Nawab Y, Baheti V. Modeling and analysis of the creep behavior of jute/green epoxy composites incorporated with chemically treated pulverized nano/micro jute fibers. Ind Crop Prod. 2016;84:230-40.

[2] Lu T, Jiang M, Jiang Z, Hui D, Wang Z, Zhou Z. Effect of surface modification of bamboo cellulose fibers on mechanical properties of cellulose/epoxy composites. Compos Part B: Eng. 2013;51:28-34.

[3] Ku H, Wang H, Pattarachaiyakoop N, Trada M. A review on the tensile properties of natural fiber reinforced polymer composites. Compos Part B: Eng. 2011;42(4):856-73.

[4] Dányádi L, Móczó J, Pukánszky B. Effect of various surface modifications of wood flour on the properties of PP/wood composites. Compos Part A: Appl Sci Manufac. 2010;41(2):199-206.

[5] Chirayil CJ, Joy J, Mathew L, Koetz J, Thomas S. Nanofibril reinforced unsaturated polyester nanocomposites: morphology, mechanical and barrier properties, viscoelastic behavior and polymer chain confinement. Ind Crop Prod. 2014;56:246-54.

[6] Cho M-J, Park B-D. Tensile and thermal properties of nanocellulose-reinforced poly (vinyl alcohol) nanocomposites. J Ind Eng Chem. 2011;17(1):36-40.

[7] Lee S-Y, Mohan DJ, Kang I-A, Doh G-H, Lee S, Han SO. Nanocellulose reinforced PVA composite films: effects of acid treatment and filler loading. Fib Polym. 2009;10(1):77-82.

[8] Dai D, Fan M, Collins P. Fabrication of nanocelluloses from hemp fibers and their application for the reinforcement of hemp fibers. Ind Crop Prod. 2013;44:192-9.

[9] Costa LMM, de Olyveira GM, Cherian BM, Leão AL, de Souza SF, Ferreira M. Bionanocomposites from electrospun PVA/pineapple nanofibers/Stryphnodendron adstringens bark extract for medical applications. Ind Crop Prod. 2013;41:198-202.

[10] Das K, Ray D, Banerjee C, Bandyopadhyay N, Sahoo S, Mohanty AK, et al. Physicomechanical and thermal properties of jute-nanofiber-reinforced biocopolyester composites. Ind Eng Chem Res. 2010;49(6):2775-82.

[11] Militký J, Jabbar A. Comparative evaluation of fiber treatments on the creep behavior of jute/green epoxy composites. Compos Part B: Eng. 2015;80:361-8.

[12] Baheti V, Militky J. Reinforcement of wet milled jute nano/micro particles in polyvinyl alcohol films. Fib Polym. 2013;14(1):133-7.

[13] Ng H-M, Sin LT, Tee T-T, Bee S-T, Hui D, Low C-Y, et al. Extraction of cellulose nanocrystals from plant sources for application as reinforcing agent in polymers. Compos Part B: Eng. 2015;75:176-200.

[14] Mukherjee A, Ganguly P, Sur D. Structural mechanics of jute: the effects of hemicellulose or lignin removal. J Text Inst. 1993;84(3):348-53.

[15] Ray D, Sarkar BK, Rana A, Bose NR. Effect of alkali treated jute fibres on composite properties. Bull Mater Sci. 2001;24(2):129-35.

[16] Beg MDH, Pickering KL. Accelerated weathering of unbleached and bleached Kraft wood fibre reinforced polypropylene composites. Polym Degrad Stab. 2008;93(10):1939-46.

[17] Terinte N, Ibbett R, Schuster KC. Overview on native cellulose and microcrystalline cellulose I structure studied by X-ray diffraction (WAXD): Comparison between measurement techniques. Lenzin Berich. 2011;89:118-31.

[18] Kale BM, Wiener J, Militky J, Rwawiire S, Mishra R, Jabbar A. Dyeing and stiffness characteristics of cellulose-coated cotton fabric. Cellul. 2016;23(1):981-92.

[19] Kale BM, Wiener J, Militky J, Rwawiire S, Mishra R, Jacob KI, et al. Coating of cellulose-TiO 2 nanoparticles on cotton fabric for durable photocatalytic self-cleaning and stiffness. Carbohyd Polym. 2016;150:107-13.

[20] Wetzel B, Rosso P, Haupert F, Friedrich K. Epoxy nanocomposites–fracture and toughening mechanisms. Eng Fract Mechan. 2006;73(16):2375-98.

[21] Alamri H, Low IM. Characterization of epoxy hybrid composites filled with cellulose fibers and nano-SiC. J Appl Polym Sci. 2012;126(S1).

[22] Zhao S, Schadler LS, Hillborg H, Auletta T. Improvements and mechanisms of fracture and fatigue properties of well-dispersed alumina/epoxy nanocomposites. Compos Sci Technol. 2008;68(14):2976-82.

[23] Sreenivasan V, Rajini N, Alavudeen A, Arumugaprabu V. Dynamic mechanical and thermo-gravimetric analysis of Sansevieria cylindrica/polyester composite: Effect of fiber length, fiber loading and chemical treatment. Compos Part B: Eng. 2015;69:76-86.

[24] Jabbar A, Militký J, Wiener J, Karahan M. Static and dynamic mechanical properties of novel treated jute/green epoxy composites. Text Res J. 2016;86(9):960-74.

[25] Pothan LA, Oommen Z, Thomas S. Dynamic mechanical analysis of banana fiber reinforced polyester composites. Compos Sci Technol. 2003;63(2):283-93.

[26] Chirayil CJ, Mathew L, Hassan P, Mozetic M, Thomas S. Rheological behaviour of nanocellulose reinforced unsaturated polyester nanocomposites. Int J Bio Macromol. 2014;69:274-81.

[27] Ray D, Sarkar B, Das S, Rana A. Dynamic mechanical and thermal analysis of vinylester-resin-matrix composites reinforced with untreated and alkali-treated jute fibres. Compos Sci Technol. 2002;62(7):911-7.

[28] Kargarzadeh H, Sheltami RM, Ahmad I, Abdullah I, Dufresne A. Cellulose nanocrystal: A promising toughening agent for unsaturated polyester nanocomposite. Polym. 2015;56:346-57.

[29] Lu J, Wang T, Drzal LT. Preparation and properties of microfibrillated cellulose polyvinyl alcohol composite materials. Compos Part A: Appl Sci Manufac. 2008;39(5):738-46.

[30] Samir MASA, Alloin F, Sanchez J-Y, Dufresne A. Cellulose nanocrystals reinforced poly (oxyethylene). Polym. 2004;45(12):4149-57.

[31] Raquez J-M, Murena Y, Goffin A-L, Habibi Y, Ruelle B, DeBuyl F, et al. Surface-modification of cellulose nanowhiskers and their use as nanoreinforcers into polylactide: a sustainably-integrated approach. Compos Sci Technol. 2012;72(5):544-9.

[32] Karaduman Y, Onal L. Dynamic mechanical and thermal properties of enzyme-treated jute/polyester composites. J Compos Mater. 2013;47(19):2361-70.

[33] Romanzini D, Ornaghi HL, Amico SC, Zattera AJ. Influence of fiber hybridization on the dynamic mechanical properties of glass/ramie fiber-reinforced polyester composites. J Reinf Plast Comp. 2012;31(23):1652-61.

[34] Sudhir K, Gautam S, Aru C. Dynamic mechanical analysis of randomly oriented short bagasse/coir hybrid fiber reinforced epoxy Novolc composites. Fib Polym. 2011;12(4):506-13.

[35] Martínez-Hernández A, Velasco-Santos C, De-Icaza M, Castano VM. Dynamical–mechanical and thermal analysis of polymeric composites reinforced with keratin biofibers from chicken feathers. Compos Part B: Eng. 2007;38(3):405-10.

[36] Akay M. Aspects of dynamic mechanical analysis in polymeric composites. Compos Sci Technol. 1993;47(4):419-23.

[37] Brunner A, Necola A, Rees M, Gasser P, Kornmann X, Thomann R, et al. The influence of silicate-based nano-filler on the fracture toughness of epoxy resin. Eng Fract Mechan. 2006;73(16):2336-45.

[38] Dong S, Gauvin R. Application of dynamic mechanical analysis for the study of the interfacial region in carbon fiber/epoxy composite materials. Polym Compos. 1993;14(5):414-20.

[39] Júnior JHSA, Júnior HLO, Amico SC, Amado FDR. Study of hybrid intralaminate curaua/glass composites. Mater Des. 2012;42:111-7.

Figure captions

Fig. 1. SENB (single edge notch bending) specimen and fixture dimensions for flexural test (dimensions in mm).

Fig. 2. SEM images of jute fibers (a) untreated, (b) alkali treated, (c) bleached, (d) milled, (e) and (f) acid hydrolyzed.

Fig. 3. (a) FE-SEM image of jute cellulose nanofibrils. (b) Histogram of size distribution of cellulose nanofibrils.

Fig. 4. Surface morphology of jute fabric coated with; (a) 0 wt%, (b) 2 wt%, (c) 5 wt%, (d) 10 wt% of nanocellulose suspensions.

Fig. 5. X-ray diffraction patterns of untreated, bleached jute fibers and jute cellulose nanofibrils.

Fig. 6. (a) Tensile stress-strain curves and (b) tensile strength and modulus of uncoated and nanocellulose coated jute composites.

Fig. 7. Flexural strength and modulus of uncoated and nanocellulose coated jute/green epoxy composites.

Fig. 8. (a) Typical K_Q vs. displacement curves and (b) fracture toughness (K_{1c}) of uncoated and nanocellulose coated jute/green epoxy composites.

Fig. 9. Fracture surface morphology of jute/green epoxy composites; (a) CF0, (b) CF3, (c) CF5 and (d) CF10.

Fig. 10. Fracture surfaces in the matrix region of jute/green composites; (a) CF0, (b) CF3, (c) CF5 and (d) CF10.

Fig. 11. Storage modulus versus temperature for uncoated and nanocellulose coated jute/green epoxy composites.

Fig. 12. Variation of storage modulus (E') at different temperatures for uncoated and nanocellulose coated jute/green epoxy composites.

Fig. 13. Loss modulus versus temperature for uncoated and nanocellulose coated jute/green epoxy composites.

Fig. 14. tanδ versus temperature for uncoated and nanocellulose coated jute/green epoxy composites.

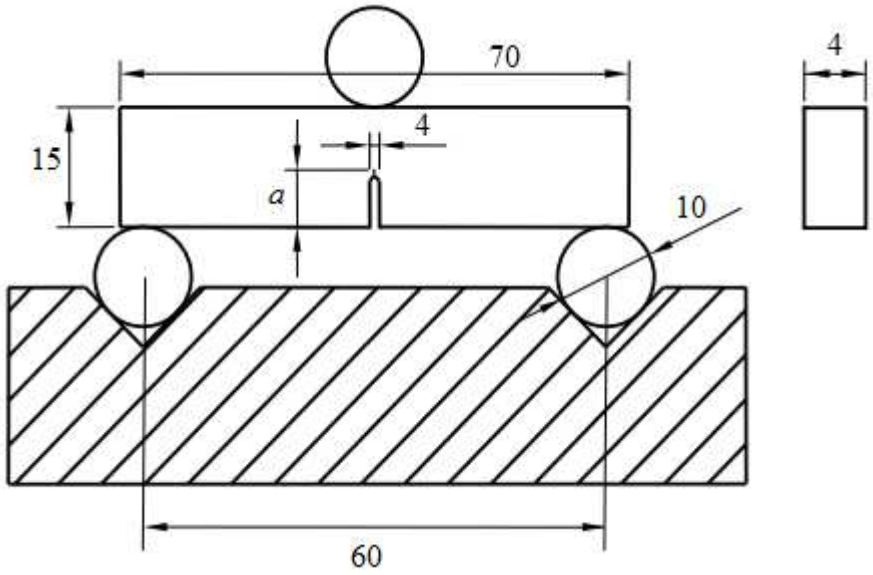

Fig. 1

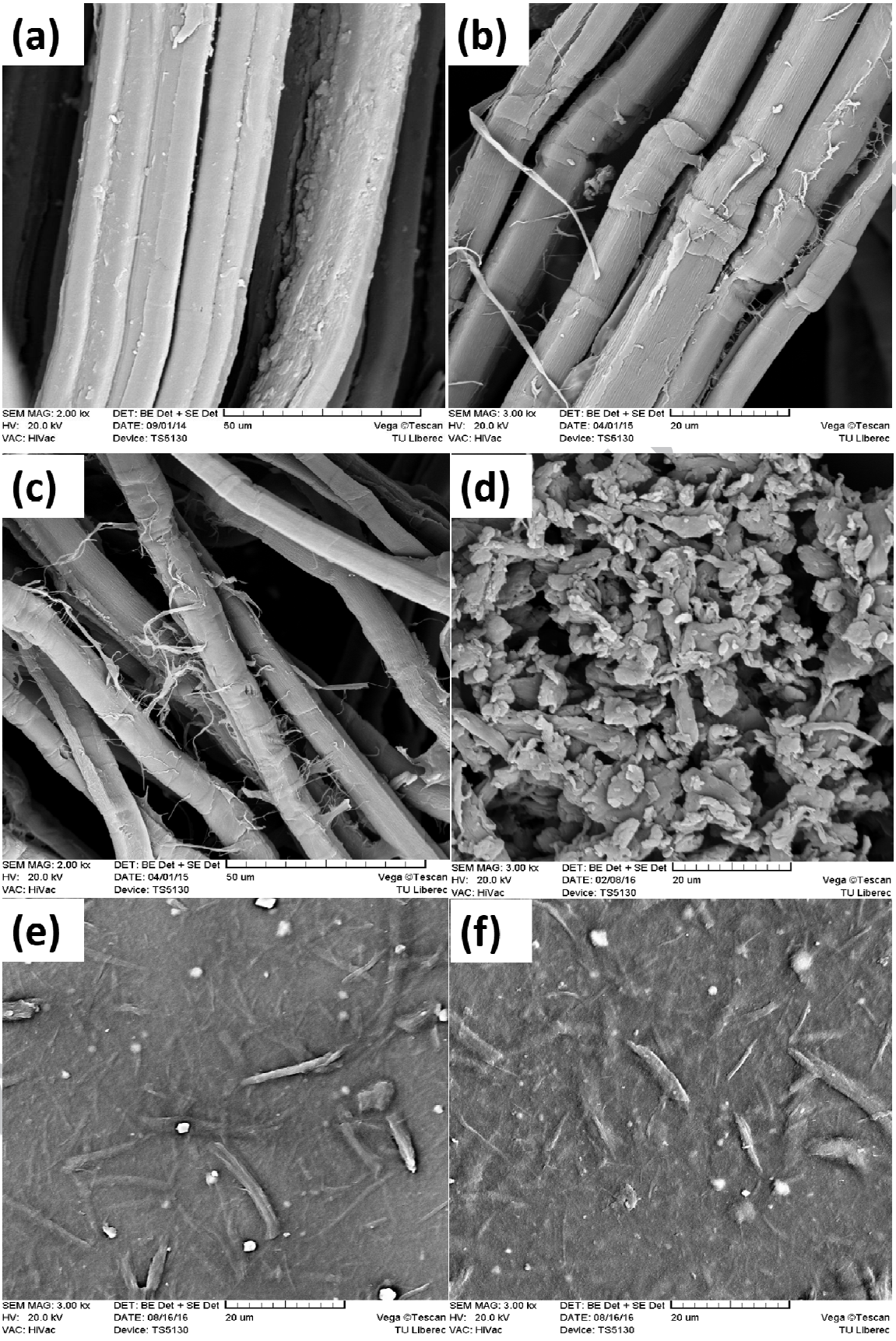
(a)
SEM MAG: 2.00 kx
HV: 20.0 kV
VAC: HiVac
DET: BE Det + SE Det
DATE: 09/01/14
Device: TS5130
50 um
Vega ©Tescan
TU Liberec
(b)
SEM MAG: 3.00 kx
HV: 20.0 kV
VAC: HiVac
DET: BE Det + SE Det
DATE: 04/01/15
Device: TS5130
20 um
Vega ©Tescan
TU Liberec
(c)
SEM MAG: 2.00 kx
HV: 20.0 kV
VAC: HiVac
DET: BE Det + SE Det
DATE: 04/01/15
Device: TS5130
50 um
Vega ©Tescan
TU Liberec
(d)
SEM MAG: 3.00 kx
HV: 20.0 kV
VAC: HiVac
DET: BE Det + SE Det
DATE: 02/08/16
Device: TS5130
20 um
Vega ©Tescan
TU Liberec
(e)
SEM MAG: 3.00 kx
HV: 20.0 kV
VAC: HiVac
DET: BE Det + SE Det
DATE: 08/16/16
Device: TS5130
20 um
Vega ©Tescan
TU Liberec
(f)
SEM MAG: 3.00 kx
HV: 20.0 kV
VAC: HiVac
DET: BE Det + SE Det
DATE: 08/16/16
Device: TS5130
20 um
Vega ©Tescan
TU Liberec

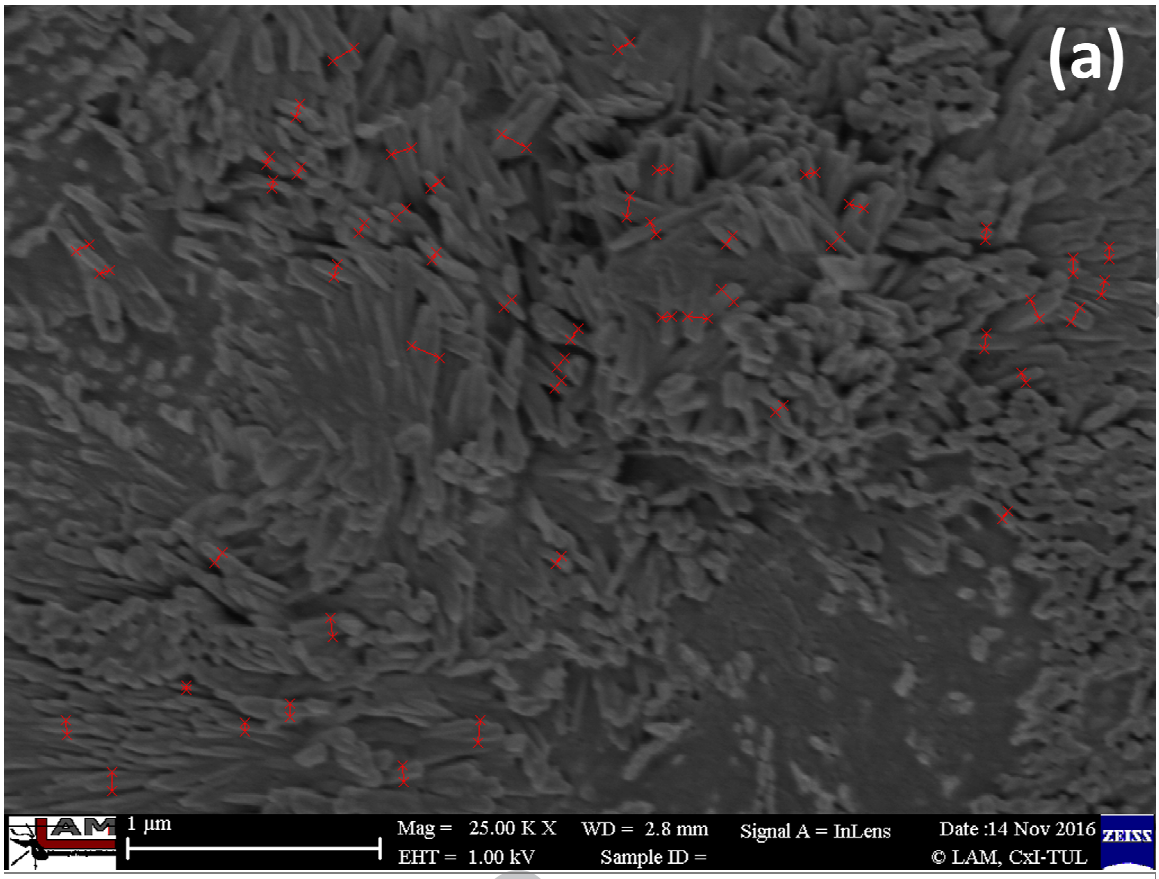

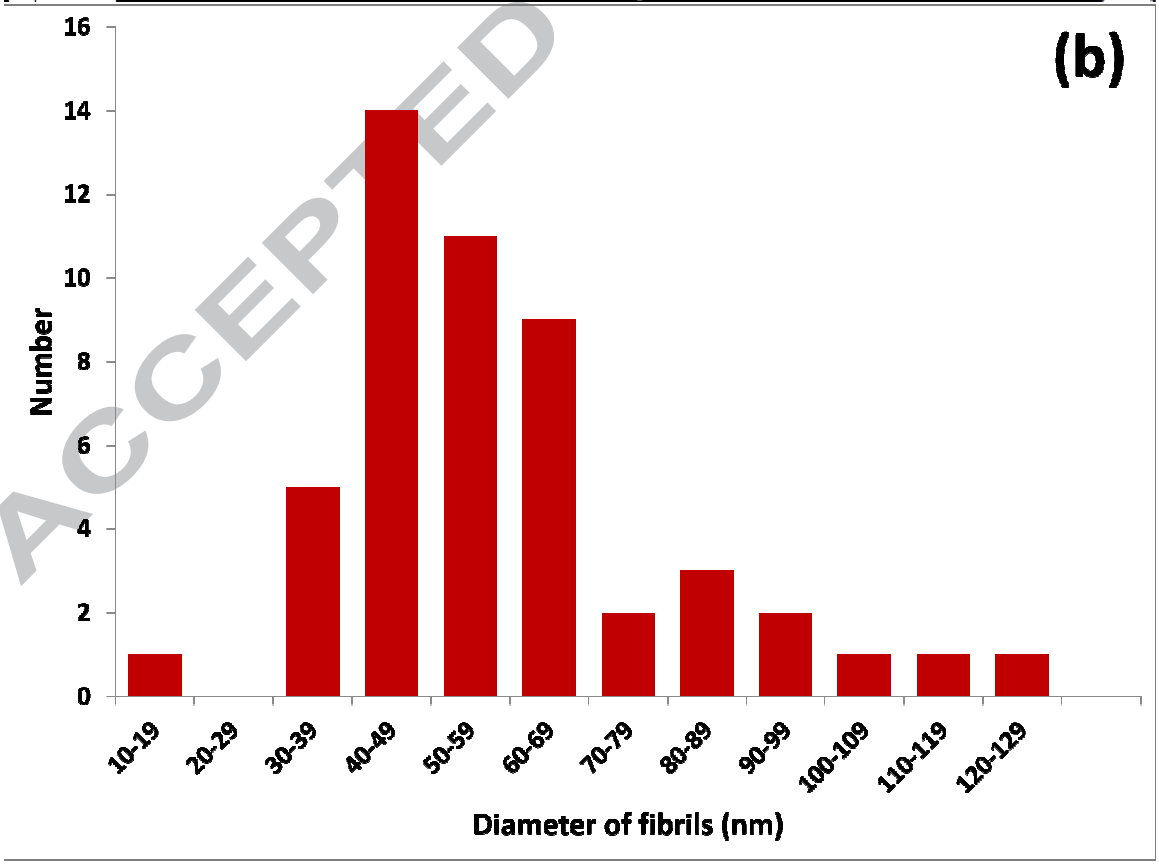

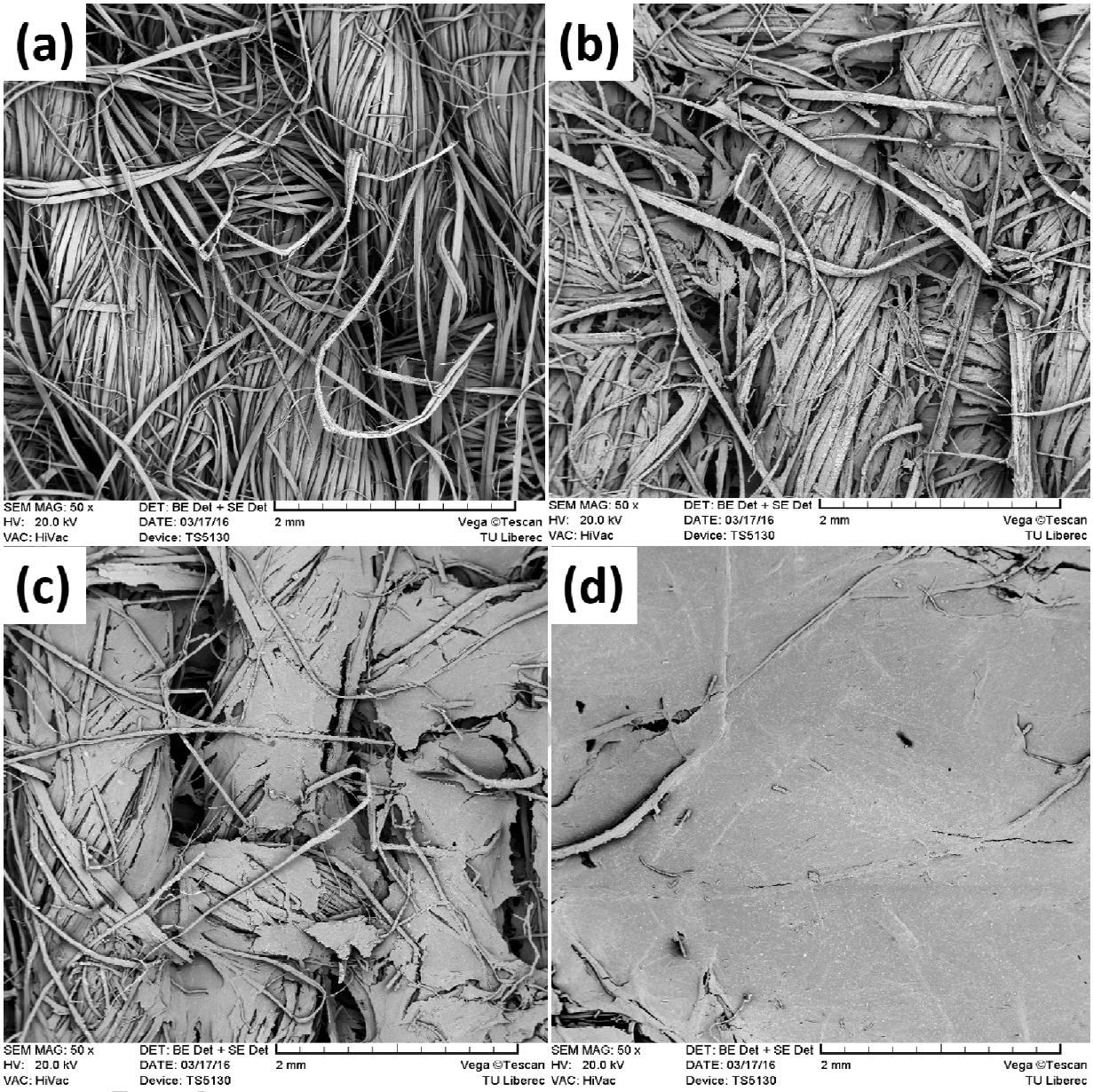
(a)
SEM MAG: 50 x
HV: 20.0 kV
VAC: HiVac
DET: BE Det + SE Det
DATE: 03/17/16
Device: TS5130
2 mm
Vega ©Tescan
TU Liberec
(b)
SEM MAG: 50 x
HV: 20.0 kV
VAC: HiVac
DET: BE Det + SE Det
DATE: 03/17/16
Device: TS5130
2 mm
Vega ©Tescan
TU Liberec
(c)
SEM MAG: 50 x
HV: 20.0 kV
VAC: HiVac
DET: BE Det + SE Det
DATE: 03/17/16
Device: TS5130
2 mm
Vega ©Tescan
TU Liberec
(d)
SEM MAG: 50 x
HV: 20.0 kV
VAC: HiVac
DET: BE Det + SE Det
DATE: 03/17/16
Device: TS5130
2 mm
Vega ©Tescan
TU Liberec

Fig. 4

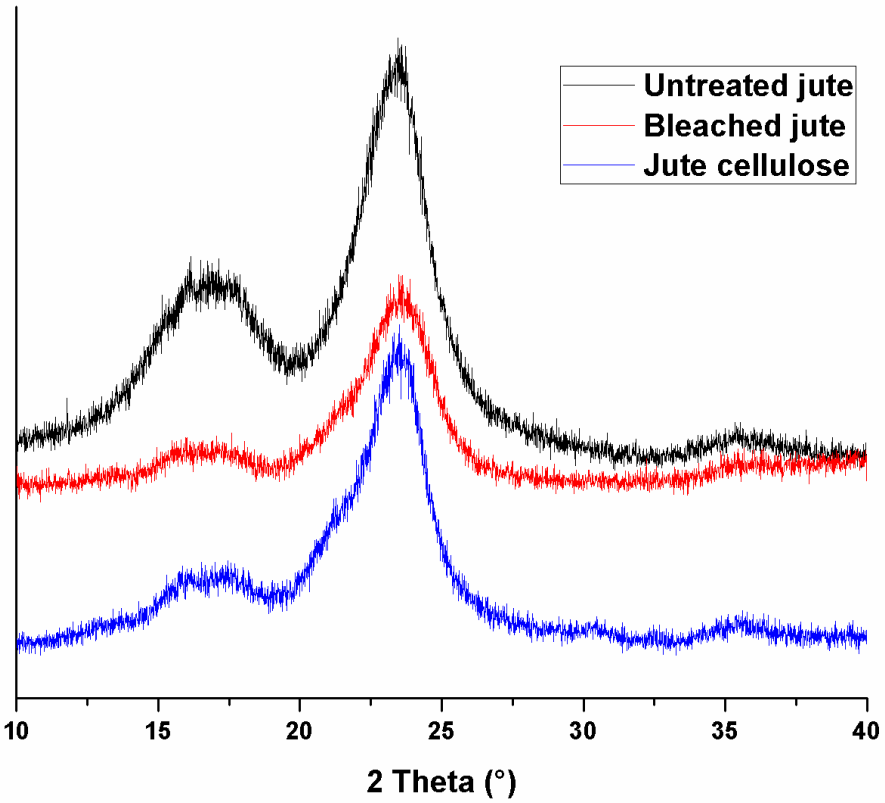

Fig. 5

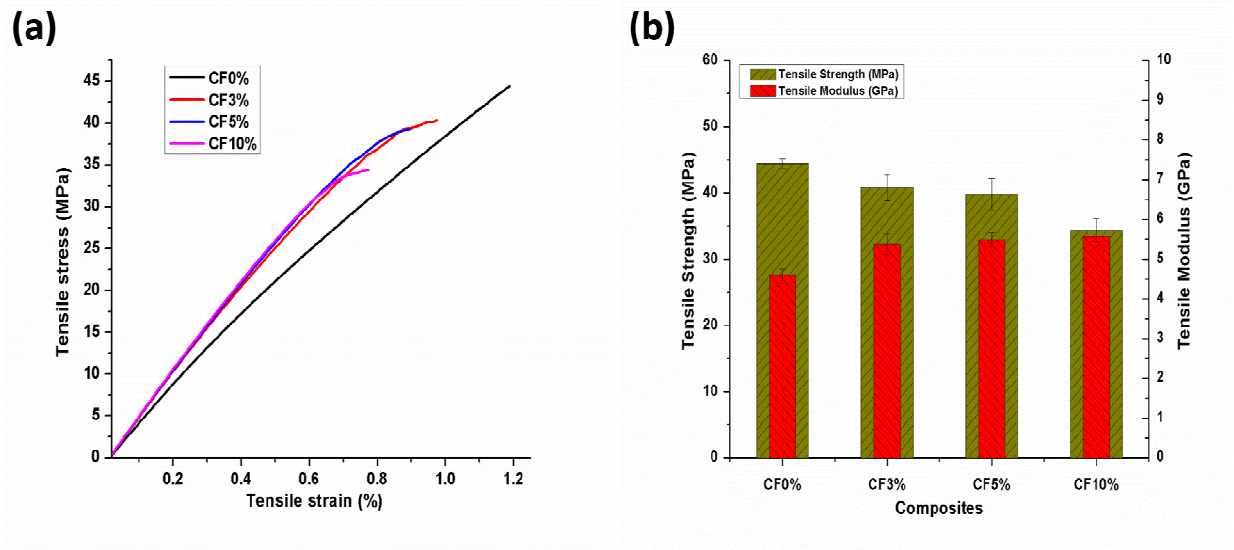

Fig. 6

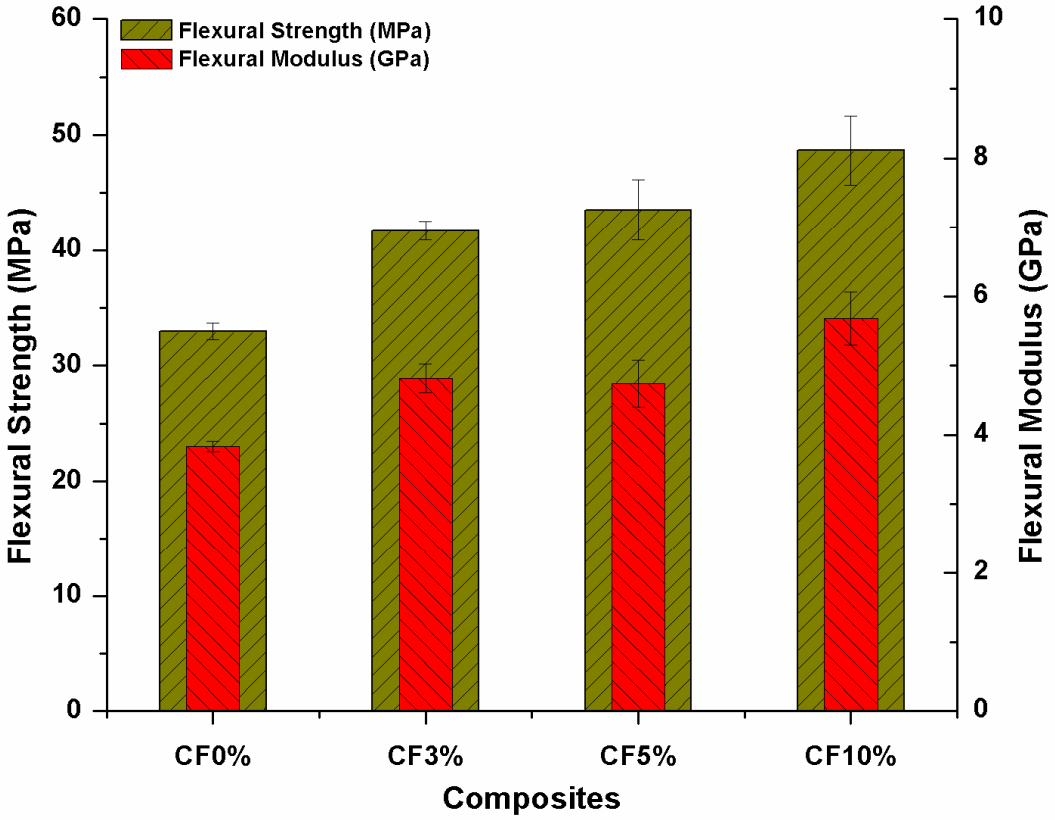

Fig. 7

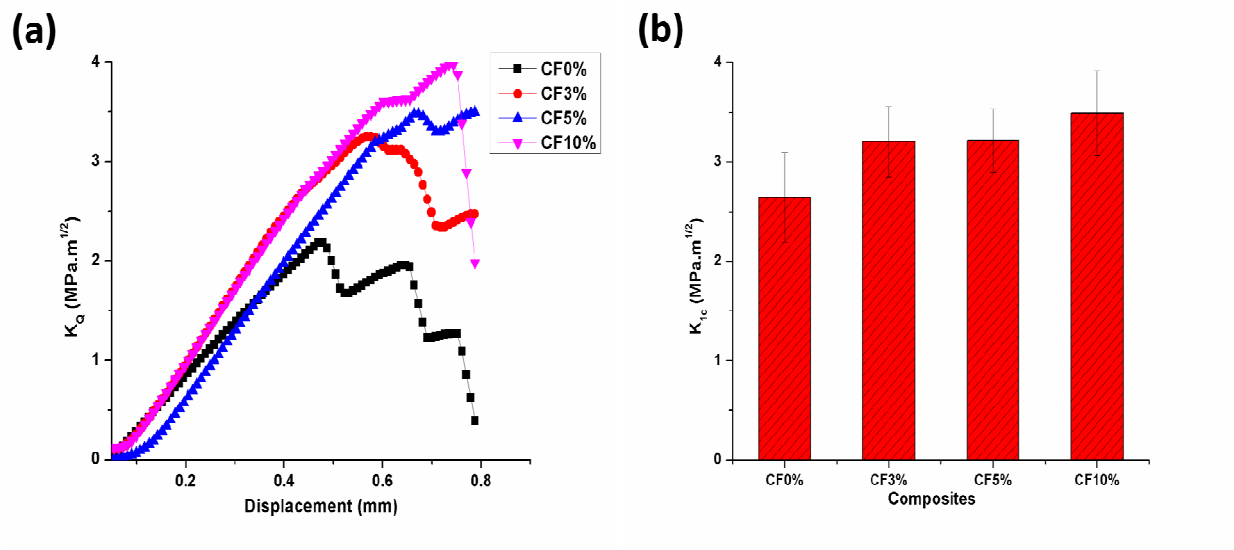

Fig. 8

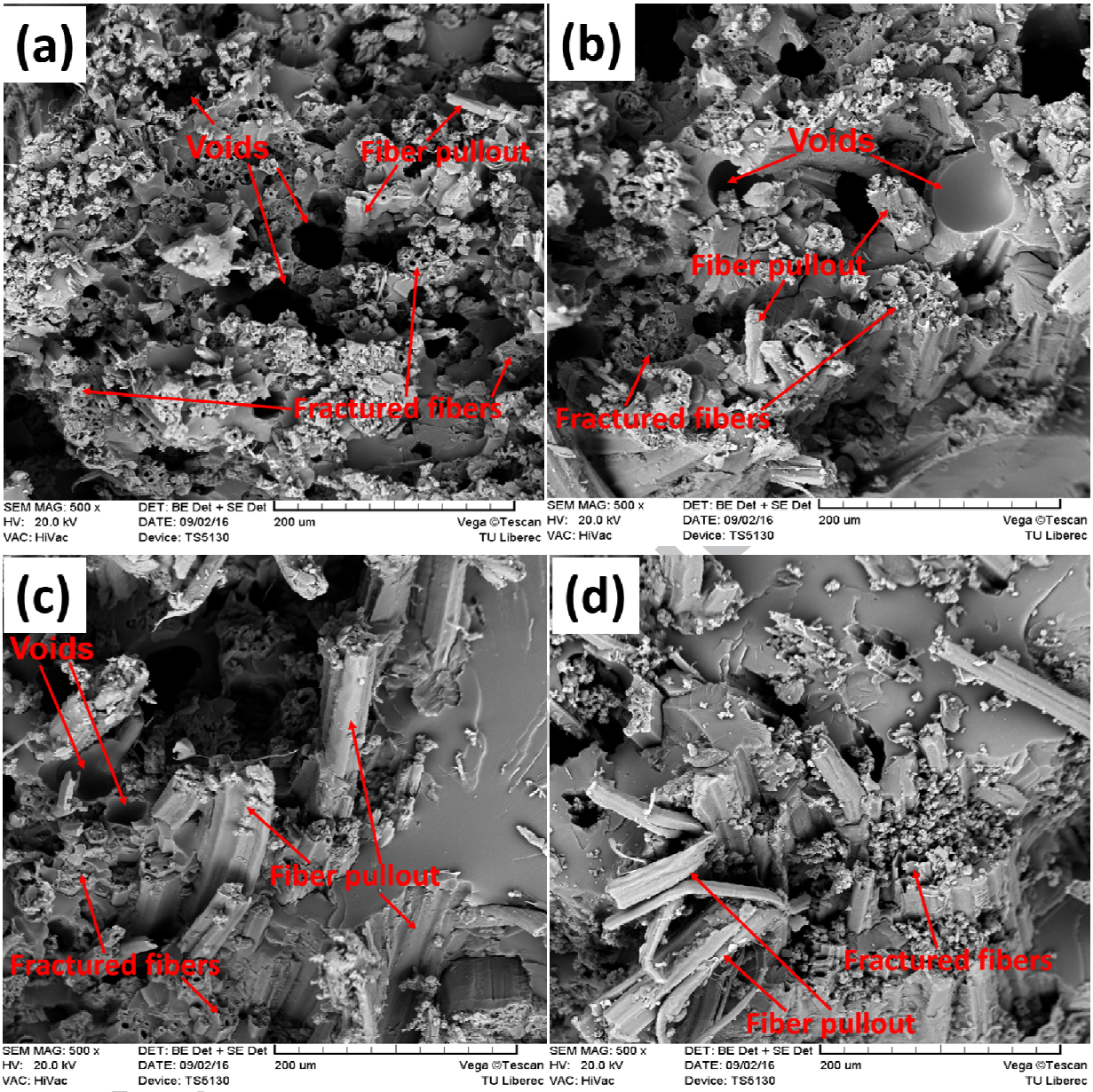
(a)
Voids
Fiber pullout
Fractured fibers
SEM MAG: 500 x
HV: 20.0 kV
VAC: HiVac
DET: BE Det + SE Det
DATE: 09/02/16
Device: TS5130
200 um
Vega ©Tescan
TU Liberec
(b)
Voids
Fiber pullout
Fractured fibers
SEM MAG: 500 x
HV: 20.0 kV
VAC: HiVac
DET: BE Det + SE Det
DATE: 09/02/16
Device: TS5130
200 um
Vega ©Tescan
TU Liberec
(c)
Voids
Fiber pullout
Fractured fibers
SEM MAG: 500 x
HV: 20.0 kV
VAC: HiVac
DET: BE Det + SE Det
DATE: 09/02/16
Device: TS5130
200 um
Vega ©Tescan
TU Liberec
(d)
Fractured fibers
Fiber pullout
SEM MAG: 500 x
HV: 20.0 kV
VAC: HiVac
DET: BE Det + SE Det
DATE: 09/02/16
Device: TS5130
200 um
Vega ©Tescan
TU Liberec

Fig. 9

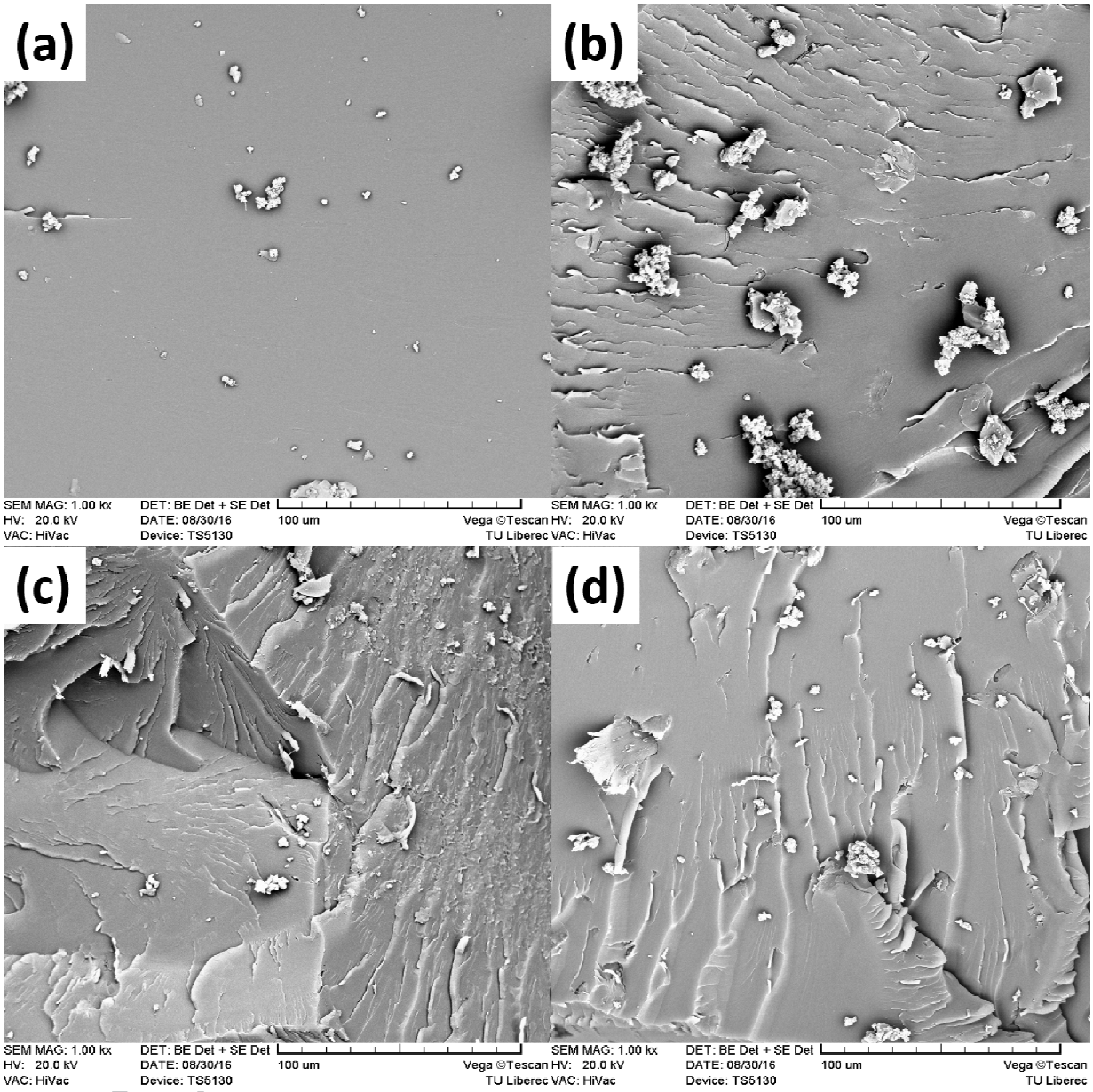
(a)
(b)
(c)
(d)
SEM MAG: 1.00 kx
HV: 20.0 kV
VAC: HiVac
DET: BE Det + SE Det
DATE: 08/30/16
Device: TS5130
100 um
Vega ©Tescan
TU Liberec

Fig. 10

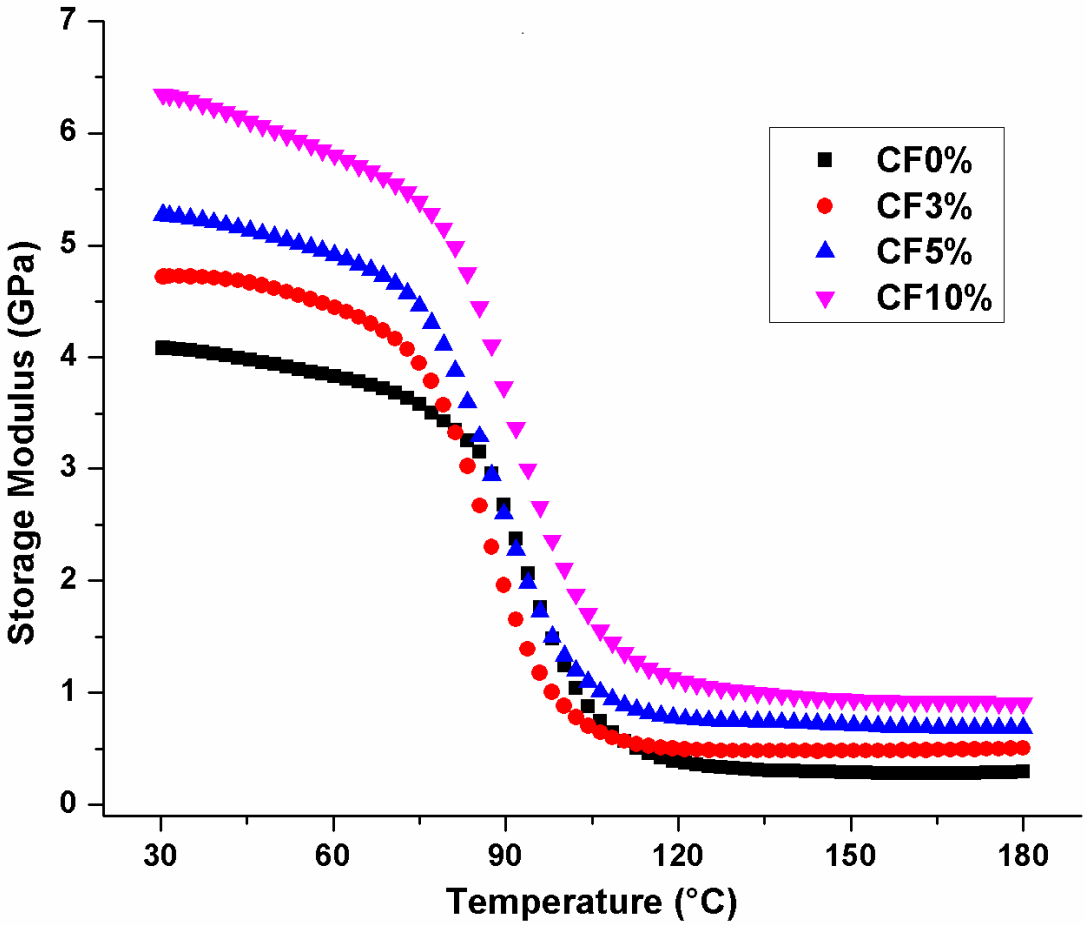

Fig. 11

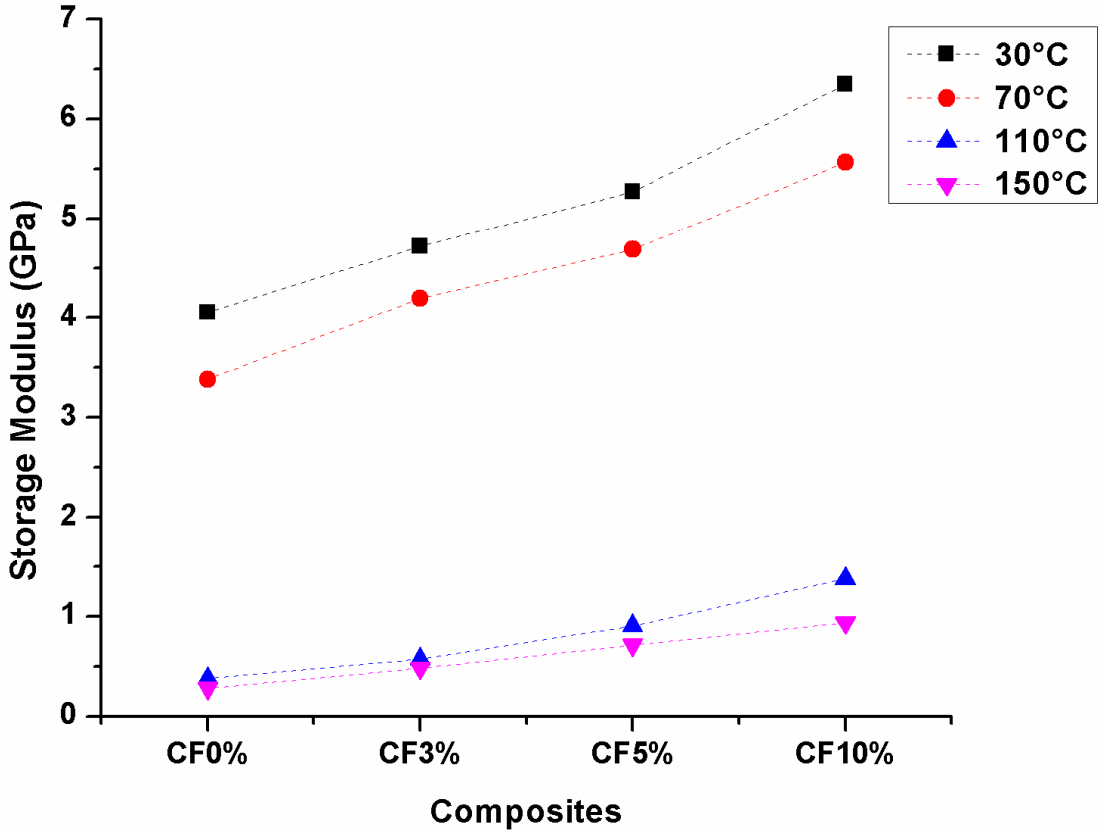

Fig. 12

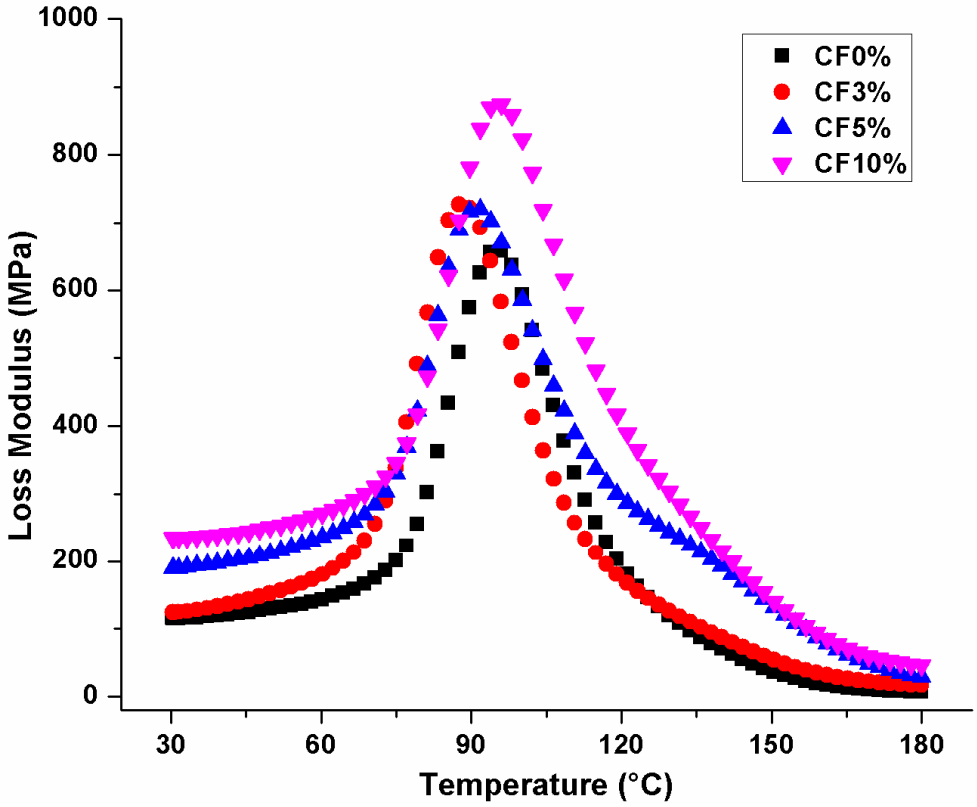

Fig. 13

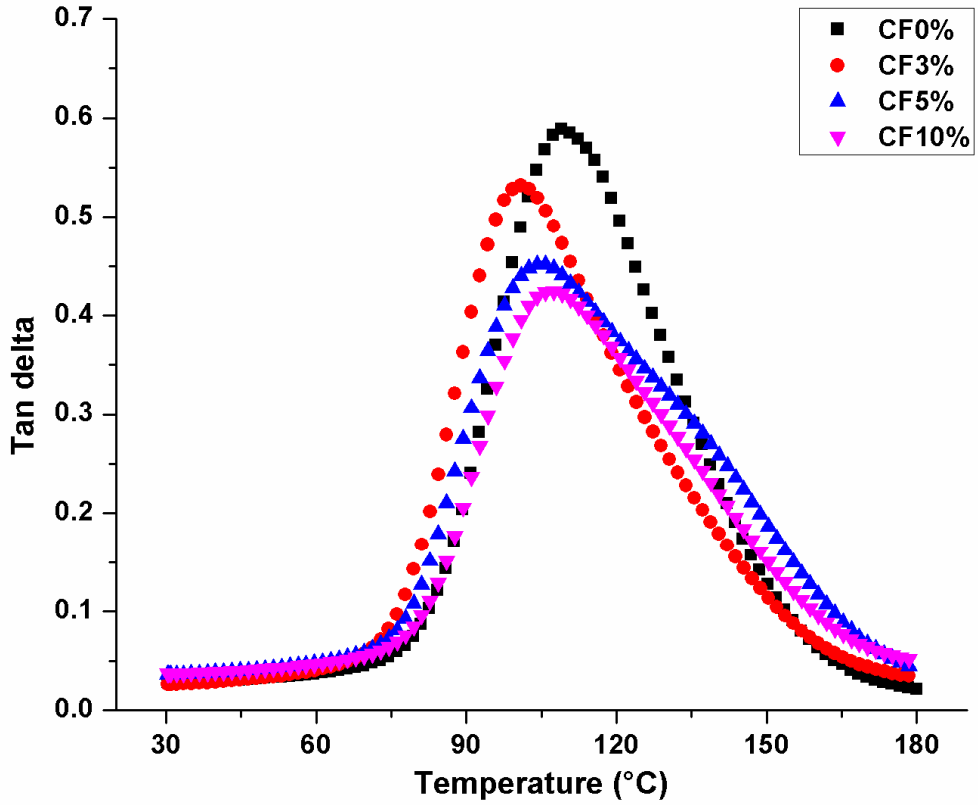

Fig. 14

Table 1. T_g values obtained from E'' curves and tanδ peak height of composites.

Composites	T_g from E''_{max} curve (°C)	Tanδ peak height
CF0	95.17	0.59
CF3	88.19	0.53
CF5	91.04	0.45
CF10	95.36	0.42